agriculture

MDPI

Article

The Adsorption Characteristics of Phosphorus-Modified Corn Stover Biochar on Lead and Cadmium

Lina Zhou, Lin Chen, Yuqing Zhang, Yu Zhang, Zhifan Li, Kun Yang and Limei Chen *

College of Engineering and Technology, Jilin Agricultural University, Changchun 130118, China; zhoulina976430@163.com (L.Z.); 18478362986@163.com (L.C.); 13756676331@163.com (Y.Z.); 13756705586@163.com (Y.Z.); 18743377295@163.com (Z.L.); yangkun2000@163.com (K.Y.)
* Correspondence: chenlimei@jlau.edu.cn

Abstract: In order to achieve the purpose of efficiently removing lead and cadmium as the main heavy metals from wastewater, this paper explores the adsorption properties of cadmium ions and lead ions on biochar under different modified conditions prepared from corn stalks as raw materials and potassium phosphate as surface modifiers. Before preparing biochar (BC), the mass ratios of 1:1 and 1:2 (corn stalks to potassium phosphate) were used for pre-modification, and the oxygen-restricted pyrolysis processes of 350 °C, 550 °C and 750 °C were used for treatment. The study discussed the individual and composite adsorption effects of biochar on Pb^{2+} and Cd^{2+} under different conditions. The experimental results show that phosphorus modification has changed the physical and chemical properties of the original biochar. Among them, the biochar (2PBC550) with an impregnation ratio of 1:2 and a pyrolysis temperature of 550 °C (2PBC550) exhibits excellent adsorption properties. When the pH of the simulated wastewater is 5 and the amount of adsorbent is 30 $mg \cdot L^{-1}$, the maximum adsorption capacity of Pb^{2+} and Cd^{2+} is 145.48 $mg \cdot g^{-1}$ and 14.533 $mg \cdot g^{-1}$, respectively, which are 6.46 times and 3.67 times of the original biochar. The Pb^{2+} and Cd^{2+} adsorption data of 2PBC550 fit well with the quasi-secondary dynamics and Langmuir isothermal models, indicating that the adsorption process is controlled by single-layer chemical adsorption. In the composite metal system of Pb^{2+} and Cd^{2+}, 2PBC550 exhibits a stronger affinity for Pb^{2+} than Cd^{2+}. Through the analysis of characterization methods such as SEM, FTIR, XRD and XPS, it is proved that the adsorption of Pb^{2+} and Cd^{2+} by 2PBC550 is due to precipitation, complexation and π electron interaction. Therefore, 2PBC550 shows great application potential in the repair of wastewater containing Pb^{2+} or Cd^{2+}.

Keywords: phosphorus-rich biochar; corn stalks; heavy metals; adsorption mechanism

Citation: Zhou, L.; Chen, L.; Zhang, Y.; Zhang, Y.; Li, Z.; Yang, K.; Chen, L. The Adsorption Characteristics of Phosphorus-Modified Corn Stover Biochar on Lead and Cadmium. *Agriculture* **2024**, *14*, 1118. https://doi.org/10.3390/agriculture14071118

Academic Editors: Jose Joaquin Ramos-Miras and Daniele Del Buono

Received: 20 May 2024
Revised: 4 July 2024
Accepted: 7 July 2024
Published: 11 July 2024

1. Introduction

With the advancement of industrial modernization, lead (Pb^{2+}) and cadmium (Cd^{2+}) pollution in metallurgy, mining, electroplating, agriculture and other fields is becoming more and more serious. The heavy metal polluted wastewater produced in these industries will enter and exit water bodies and soil environments through different channels, and the metals lead and cadmium have the characteristics of high chemical activity and high fluidity [1,2]. They have long-lasting toxicity and high toxicity in the environment, posing a serious threat to human health and the environment [3]. Currently, the major treatments for heavy metals are chemical precipitation, electric flocculation, adsorption, ion exchange and membrane separation; of which adsorption is a more economical and efficient method in heavy metal treatment [4,5].

At present, despite the extensive use of adsorbents such as activated carbon, metal-organic skeleton nano-particles and mesoporous composite materials in extracting heavy metals from sewage, large-scale sewage treatment faces limitations due to its intricate composition, high expense, or inadequate removal efficiency. Biochar is an adsorbent prepared by pyrolysis of biomass as raw material under oxygen-free or oxygen-restricted conditions.

It has been demonstrated that biochar efficiently extracts heavy metals from water through adsorption [6] and—owing to its benefits of being affordable, readily available, broadly sourced, and eco-friendly in adsorption—it has received widespread attention [7]. At present, research indicates that biochar exhibits significant absorption capabilities of heavy metals in solutions and even in dilute solutions; but almost all primitive biochar lacks the high adsorption capacity and anti-interference ability typical of heavy metals [8]. Consequently, researchers have innovated diverse alteration techniques to enhance biochar's adsorption abilities—including physical changes such as ball milling and UV light exposure and chemical alterations such as acid-base and load metal changes—to boost biochar's absorption potential. Research has demonstrated that, unlike the traditional modification of post-carbonized substances, the modification of pre-carbonized biomass can also significantly improve the performance of biochar [9,10]. For example, Bakshi et al. used magnetite to prepare a zero-valent iron biochar complex material by co-pyrolysis using magnetite after pretreatment of sawdust biomass, and its adsorption of arsenic in water increased from 1.42 $mg \cdot g^{-1}$ to 15.58 $mg \cdot g^{-1}$ [11]. Son et al. used iron chloride to pretreatment the biomass of large algae and then pyrolysis to improve its heavy metal adsorption capacity [12]. The modified process of pretreatment of biological substances and then pyrolysis can produce biochar with high adsorption of heavy metals.

Studies have shown that when soluble phosphate (P) is added to wastewater containing heavy metals, it can promote the formation of low-solubility metal phosphate precipitation of heavy metals; thereby effectively removing heavy metals from the aqueous solution [2,13]. However, due to phosphate being completely soluble in water, its application in wastewater is subject to certain restrictions. To this end, some studies have proposed loading phosphates on biochar to enhance the surface chemical properties of biochar and improve the adsorption of heavy metals in wastewater. In recent years, the use of P-containing reagents such as phosphate to modify biochar as an adsorbent has received widespread attention [14]. Zhang et al. used phosphate Na_2HPO_4 to modify the active bamboo biomass and prepared biochar by pyrolysis. Compared with the original biochar, the Cd^{2+} removal rate increased by 85.78% [15]. Gao et al. used the proportional co-pyrolysis of rapeseed straw and potassium dihydrogen phosphate (KH_2PO_4); the adsorption of the modified biochar Pb^{2+} in the aqueous solution was 8.5 times higher than that of the original rapeseed straw biochar [16]. Zhou et al. used phosphoric acid to modify banana peel biochar, so that the surface of the biochar was loaded with phosphorus functional groups, thereby significantly enhancing the adsorption capacity of Pb^{2+} [17]. The above research results show that the surface properties of biochar are improved by first modifying the biomass with P-containing substances and then pyrolysis, which is one of the effective methods of adsorbing Pb^{2+} and Cd^{2+} in wastewater.

Compared with other chemicals, potassium phosphate has the advantages of low pollution and high safety. At the same time, the K^+ ions in various phosphorus reagents have an "etching" effect, which can promote the formation of biochar pores and increase the phosphorus load; thereby improving the adsorption capacity of biochar to heavy metals [18]. Corn stalks are a cost-effective and lignocellulose-rich material, which is an ideal choice for biochar precursor. After being modified and carbonized, they have the potential to remove heavy metals from aqueous solutions. At the same time, Northeast China has extremely rich corn stalk resources. With the continuous expansion of corn acreage in Northeast China, the amount of corn stalks that can be collected has increased significantly. If it is burned on the spot, it will not only pollute the environment, but also cause a waste of potential biomass resources. The rational development and utilization of corn stalks to improve their comprehensive utilization level has always been a hot topic for scholars at home and abroad [19].

In summary, this paper carried out the modification of corn stalk biomass by potassium phosphate, and then pyrolysis to prepare phosphorus-modified biochar; the adsorption characteristics of phosphorus-modified biochar in Pb^{2+}, Cd^{2+} and Pb^{2+} and Cd^{2+} composite contaminated solutions were studied through adsorption experiments; phosphorus-

modified biochar was characterized and analyzed by material characterization methods such as scanning electron microscope (SEM), X-ray diffractometer (XRD), X-ray photoelectronic energy spectrometer (XPS), Fourier infrared spectrometer (FTIR); and its adsorption properties and mechanism of action on adsorbed heavy metals were studied, with a view to providing a scientific basis for the resource utilization of corn stalk and the efficient treatment of heavy metal pollution.

2. Materials and Methods

2.1. Preparation and Characterization of Phosphorus-Modified Biochar

First of all, the corn stalks around Changchun were selected as the precursor in this study. After cleaning with deionized water, they were dried in a drying oven at 105 °C, and then crushed through a 20 mesh sieve with a grinder. After drying, they were placed in a sealed bag and stored for backup. In this study, potassium phosphate (analytical purity) was selected as the impregnating agent, and it was pre-modified with corn stalks according to a mass ratio of 1:1 and 2:1. First, 10 g and 20 g of potassium phosphate were mixed separately with 10 g of pretreated corn stalk powder. Then, each mixture was added to 250 mL of deionized water and stirred for 15 min to ensure thorough mixing. Subsequently, the mixtures were placed into a 60 °C constant temperature oscillating bath and stirred for 2 h, completing the process of potassium phosphate modification and optimization of corn stalks. After completing the above steps, the stirred solid–liquid mixture is filtered (0.45 μm water filter membrane), the filtered solid is rinsed with deionized water, and then the rinsed solid is placed in a drying oven at 85 °C to dry and set aside. Finally, the modified biomass is placed in the muffle furnace, the final pyrolysis temperature is set to 350 °C, 550 °C, 750 °C; and the temperature is heated at a speed of 10 °C·min^{-1}. After reaching the pyrolysis temperature, it is carbonized for 2 h, the muffle furnace is closed, and it is naturally cooled to room temperature. The resulting carbonized product is crushed and passed through a 20 mesh sieve to be tested. Biochar samples obtained under different conditions are labeled as BC550, 1BC350, 1BC550, 1BC750, 2BC350, 2BC550, 2BC750 (among them, the value in front of "BC" represents the proportion of modifier added, and the subsequent value represents the temperature of pyrolysis).

After the sample preparation is completed, the biochar sample is characterized and analyzed. The Supplementary Materials describes the name, model and test parameters of the instrument used to characterize the biochar sample.

2.2. Adsorption Experiment

2.2.1. Kinetic Adsorption

$Pb(NO_3)_2$ and $Cd(NO_3)_2{\cdot}4H_2O$ were dissolved in 0.01 mol·L^{-1} $NaNO_3$ solution as the background electrolyte to prepare 200 mg·L^{-1} Pb^{2+} solution and 20 mg·L^{-1} Cd^{2+} solution. The pH of the initial solution of Pb^{2+} and Cd^{2+} was adjusted with 0.1 mol·L^{-1} HNO_3 or NaOH solution. A total of 30 mL of the initial Pb^{2+} (200 mg·L^{-1}) or initial Cd^{2+} (20 mg·L^{-1}) concentration was added to the 50 mL centrifuge tube, and then 30 mg of the adsorbent (biochar under different conditions) is added to the solution. Then the centrifuge tube is placed in a constant temperature oscillation box (180 r·min^{-1}) to oscillate for 30, 60, 150, 300, 450 and 600 min, respectively. After the centrifuge tube is removed at different points in time, the solution is filtered through a 0.45 μm water filter membrane. Then a flame atomic absorption spectrophotometer (TAS-986, Beijing Purkinje General Instrument Co., Ltd., Beijing, China) was used to determine the concentration of Pb^{2+} and Cd^{2+} in the filtrate.

2.2.2. Isothermal Adsorption Experiment

$Pb(NO_3)_2$ and $Cd(NO_3)_2{\cdot}4H_2O$ were dissolved in 0.01 mol·L^{-1} $NaNO_3$ solution as the background electrolyte to prepare 1000 mg·L^{-1} Pb^{2+} and Cd^{2+} stock solutions, respectively; these were then diluted to the desired concentration. The initial mass concentration of Pb^{2+} solution is 10, 50, 100, 200, 300 and 500 mg·L^{-1}; and the preliminary mass concentration of Cd^{2+} solution is 10, 20, 30, 40 and 50 mg·L^{-1}. A total of 30 mL of solution containing

different concentrations of Pb^{2+} or different concentrations of Cd^{2+} is added to a 50 mL centrifuge tube, and 30 mg of adsorbent (biochar under different conditions) is added to the solution; then the centrifuge tube is placed in a constant temperature oscillation box (180 r·min^{-1}) to oscillate for 10 h. After the centrifuge tube is removed, the solution is filtered through a 0.45 μm aqueous membrane to determine the concentration of Pb^{2+} and Cd^{2+} in the solution.

2.2.3. Competitive Adsorption

In competitive adsorption experiments, the concentration of Pb^{2+} in the composite solution is maintained at 100 mg·L^{-1}; meanwhile, the concentration of Cd^{2+} varies (with concentrations ranging from 0, 10, 30, 50, 100, 120, 150, 180, 200 to 250 mg·L^{-1}). The competitive adsorption characteristics of 2PBC550 were discussed by studying the effects of different Cd^{2+} concentrations on the adsorption of Pb^{2+} by 2PBC550. The concentration of Cd^{2+} in the composite solution is maintained at 150 mg·L^{-1}, while the concentration of Pb^{2+} varies (with concentrations ranging from 0, 10, 30, 50, 100, 120, 150, 180, 200 to 250 mg·L^{-1}). The competitive adsorption characteristics of 2PBC550 were discussed by studying the effects of different Pb^{2+} concentrations on the adsorption of Cd^{2+} by 2PBC550.

2.2.4. Effect of Initial pH

We discussed the effects of BC550 and 2PBC550 on the adsorption capacity of Pb^{2+} and Cd^{2+} under different pH (2~8) conditions. All other steps are the same as Section 2.2.1.

Considering that the unmodified biochar (BC550) has the best adsorption effect in the pre-experiment (from Supplementary Materials in Figure S1), it is used as a control material.

2.3. Analysis Method

Adsorption capacity (Q_e) (1) and removal efficiency (2):

$$Q_e = \frac{(C_0 - C_e)V}{m} \quad (1)$$

$$\text{Removal efficiency} = \frac{C_0 - C_e}{C_0} \times 100\% \quad (2)$$

where: Q_e is the unit adsorption amount of heavy metal ions by biochar at adsorption equilibrium, (mg·g^{-1}); C_0 and C_e are the initial concentration of the metal solution and the concentration at adsorption equilibrium, (mg·L^{-1}); V is the volume of the metal solution, (L); m is the amount of biochar added, (g).

The quasi-primary kinetic equation (PFO) (3) and quasi-secondary kinetic equation (PSO) (4) are used to fit the adsorption kinetic data:

$$Q_t = Q_{e,1}\left(1 - e^{-k_1 t}\right) \quad (3)$$

$$Q_t = \frac{Q_{e,2}^2 k_2 t}{1 + Q_{e,2} k_2 t} \quad (4)$$

where: Q_t is the adsorption capacity at time t, (mg·g^{-1}); $Q_{e,1}$ and k_1 are PFO constants, respectively, representing the adsorption equilibrium amount (mg·g^{-1}) and the adsorption rate constant (min^{-1}); $Q_{e,2}$ and k_2 are PSO kinetic constants, respectively, representing the adsorption equilibrium amount (mg·g^{-1}) and the adsorption rate constant (g·mg^{-1}·min^{-1}).

The Langmuir (5) and Freundlich (6) equations are used to fit the adsorption isothermal data:

$$Q_e = \frac{Q_m K_L C_e}{1 + K_L C_e} \quad (5)$$

$$Q_e = K_F C_e^n \quad (6)$$

where: Q_e is the equilibrium adsorption capacity of heavy metal ions, $mg \cdot g^{-1}$; Q_m and K_L represent the maximum adsorption capacity ($mg \cdot g^{-1}$) and adsorption energy ($L \cdot mg^{-1}$); K_F and n represent the adsorption capacity [$mg \cdot g^{-1} \cdot (mg \cdot L^1)^{-1/n}$] and adsorption strength.

2.4. Data Analysis

All adsorption experiments were repeated 3 times, and the adsorption performance of biochar was expressed by adsorption capacity (Q_e) and removal rate. The standard deviation of adsorption was calculated by the software SPSS 20.0. The graphs were drawn using Origin 2021.

3. Results and Discussion

3.1. Structural Characterization of Biochar

3.1.1. Pore Structure of Biochar

Table 1 shows the specific surface area (SSA) and pore structure parameters of biochar under different modification conditions. From Table 1, the SSA of the biochar modified by potassium phosphate has been greatly improved compared to the unmodified biochar. This is because under the co-pyrolysis conditions of potassium phosphate, potassium phosphate intensifies the depolarization reaction of biomass, and the "etching" effect of potassium ions on the biochar raise the SSA and total pore capacity.

Table 1. Specific surface area and pore structure parameters of biochar.

Sample	S_{BET} ($m^2 \cdot g^{-1}$)	V_{tot} ($mL \cdot g^{-1}$)	Mean Pore Width (nm)
BC550	5.70	0.015	3.15
1PBC350	29.92	0.014	0.69
1PBC550	277.77	0.246	6.82
1PBC750	208.80	0.110	2.13
2PBC350	22.90	0.034	2.51
2PBC550	272.27	0.162	3.48
2PBC750	190.87	0.731	7.20

At the same pyrolysis final temperature (550 °C), it is noteworthy that modified biochar with a lower impregnation ratio exhibits a significantly greater SSA when compared to its highly impregnated counterpart. This is because the higher impregnation ratio allows potassium phosphate to fully cover and fill the surface of the biomass and its own pores, obstructing the formation of pore structure of biochar. For biochar with relatively low degree of impregnation, potassium phosphate fails to fully fill all the pores of the biomass, which makes the biomass structure more fluffy after modification; this is conducive to pore-making, and the subsequent depolarization reaction is fully carried out to help it obtain a porous structure, which increases the SSA.

At the same impregnation ratio (1:2), the SSA of the modified biochar at different pyrolysis final temperature is compared with the potassium phosphate modified biochar with a pyrolysis final temperature of 350 °C; the surface area is only 22.90 $m^2 \cdot g^{-1}$, and the results showed that the SSA area potassium phosphate modified biochar was 272.27 $m^2 \cdot g^{-1}$ and 190.87 $m^2 \cdot g^{-1}$ at 550 °C and 750 °C, respectively, with the increment of the pyrolysis final temperature. It has been found that the SSA is the largest when it reaches 550 °C, and it drops at the final temperature of pyrolysis at 750 °C. This is because the increase in the SSA of biochar depends on the depolarization reaction of biomass polymers, and this reaction mainly occurs from 350 °C to 550 °C. However, when the pyrolysis temperature reaches 750 °C, the temperature increases and the carbon content in the product decreases. At the same time, the dehydrogenation reaction and the intensification of the depolarization reaction will increase the release of volatile components. These factors will cause the pore structure on the surface of the biochar to collapse and clog, leading to a decrease in the SSA and pore volume.

3.1.2. Surface Structure of Biochar

The microscopic morphology and structural characteristics of biochar treated with different treatments were observed by scanning scanning electron microscopy (SEM). Figure 1 illustrates that the surfaces of unmodified BC550 and BC350 are relatively smooth, flat, and have smooth pores, but they also form obvious pores and scattered fragments on the surface. The surface of all modified biochar is rough, with off-white particles appearing. It can be clearly observed that the pore structure is damaged and clogged. Through observation, it can be seen that the density of off-white particles on the surface of biological carbon with a high impregnation ratio is higher and rougher, which match the results that the SSA of biological carbon with a high impregnation ratio is less than that of biological carbon with a low impregnation ratio, indicating that the surface load of biological carbon with a high impregnation ratio the P content is higher. With the increment of the final temperature of pyrolysis, the destruction of the pore structure of biochar can be clearly observed. From the modified biochar diagram of the final temperature of pyrolysis at 750 °C, the collapse of the biochar structure can be clearly observed, and obvious macropores appear. The increase in the proportion of macropores means that the structure of biochar deteriorates, which is in accord with the research of Yakout et al. [20,21].

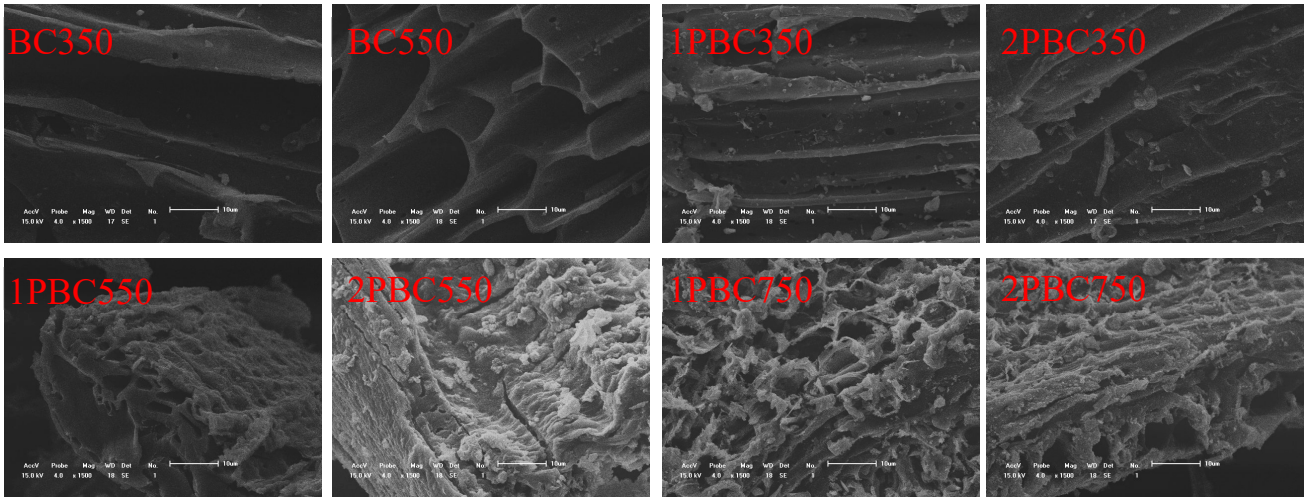

Figure 1. SEM image before and after biochar modification.

3.1.3. FTIR and XRD

The surface functional groups of biochar measured by FTIR are shown in Figure 2a. All biochar showed the presence of a wider peak near 3417 cm^{-1}, which is attributed to the telescopic vibration of the -OH group. The peak observed at 1560 cm^{-1} is caused by telescopic vibration the -COOH of the amino acid, while the characteristic peak at 1086 cm^{-1} is the telescopic vibration peak of C-O [22]. Compared with unmodified biochar, phosphorus-modified biochar has new peaks—such as the peaks at 960 cm^{-1} and 538 cm^{-1}—which are attributed to PO_4^{3-} [23]. The band located in the 692–890 cm^{-1} region is ascribed to the bending vibration of P-O-P, proving the presence of $K_4P_2O_7$ [24,25]. Additionally, the newly introduced phosphorus-containing groups, the modified biochar also showed an increase in the strength of the characteristic peaks of the hydroxyl group and the hydroxyl group. By comparing the biochar at disparate pyrolysis temperatures, it is clear that the phosphorus-containing characteristic peaks of 2PBC550 are significantly enhanced compared to the characteristic peaks of 2PBC750. This may be because the lower SSA of 2PBC750 triggers a decline in the P load of biochar. At the same time, it was found that the absorption peak of the oxygen-containing functional group of 2PBC750 is higher than that of 2PBC550; in terms of the strength, is has been weakened to a certain extent, which indicates that the higher pyrolysis final temperature is not conducive to retaining the rich

oxygen-containing functional groups on the surface of the biochar, resulting in a decrease in the ability to adsorb heavy metal ions through complex formation.

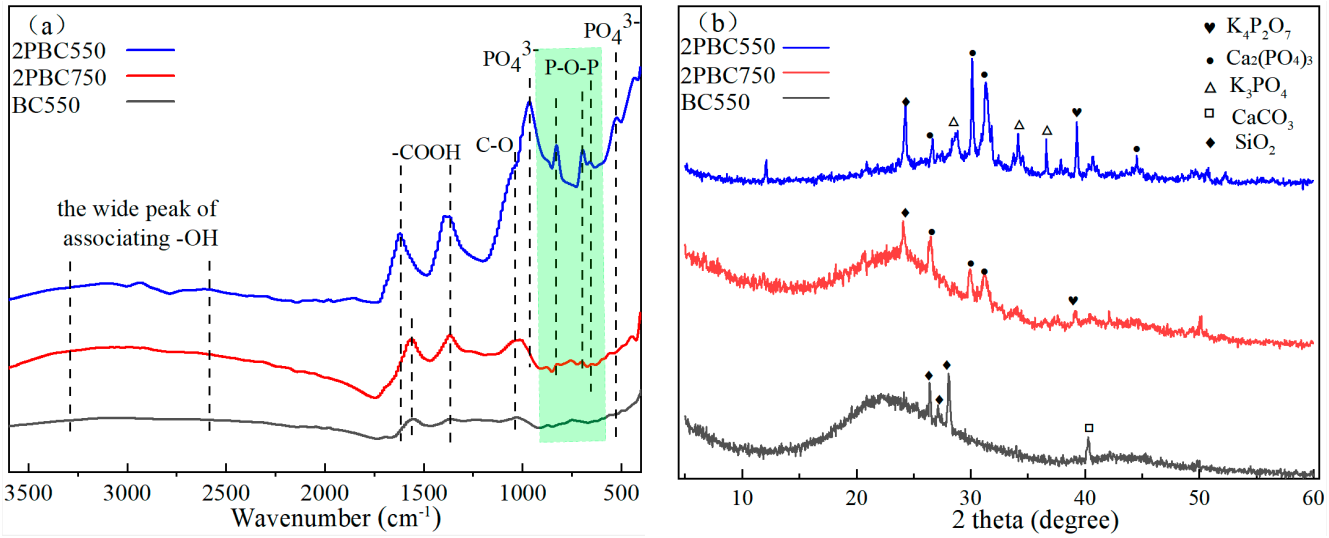

Figure 2. Infrared spectra (**a**) and XRD spectra (**b**) before and after biochar modification.

Through XRD analysis, shown in Figure 2b, the typical wide diffraction band of all biochar located at (19.80~29.79°) is amorphous carbon. A lot of K_3PO_4 diffraction peaks can be found on the surface of the modified biochar [26]. Simultaneously, a small quantity of $Ca_2(PO_4)_3$ diffraction peaks can be observed, and the presence of $K_4P_2O_7$ diffraction peaks can also be observed on the surface of the modified biochar with a final pyrolysis temperature of 550 °C and 750 °C. This may be because when the temperature is higher than 500 °C, HPO_4^{2-} thermal decomposition produces $P_2O_7^{4-}$, which is consistent with the FTIR analysis results [27].

3.2. Adsorption Experiment Analysis

3.2.1. Adsorption Dynamics

Figure 3 shows the curve of the adsorption of Pb^{2+} and Cd^{2+} in the solution by unmodified biochar and phosphorus-modified biochar over time. In the first 45 min, the phosphorus-modified biochar showed significant heavy metal adsorption capacity, and its adsorption capacity increased sharply; accounting for more than 85% of the total initial adsorption. However, as time passed to 45 min later, the adsorption of heavy metals by biochar gradually slowed down until it reached the adsorption equilibrium state. This phenomenon can be attributed to the gradual saturation of the active adsorption site on the surface of biochar. At equilibrium, the Q_e of BC550 and 2PBC550 on Pb^{2+} reached 24.5 $mg \cdot g^{-1}$ and 158.97 $mg \cdot g^{-1}$, respectively; and the Q_e of Cd^{2+} reached 4.42 $mg \cdot g^{-1}$ and 14.58 $mg \cdot g^{-1}$, respectively. From Figure 3, the adsorption of Pb^{2+} and Cd^{2+} by the five biochar species showed similar adsorption processes.

The adsorption processes of Pb^{2+} and Cd^{2+} by unmodified biochar and phosphorus-modified biochar were fitted with the PFO and PSO, respectively [28]. Table 2 shows the result of fitting. From the data in the table, it can be seen that the RMSE of the PSO is less than that of the PFO, indicating that the PSO model can better fit the data; and the PSO R_{adj}^2 is also significantly larger than the R_{adj}^2 of the PFO model, and its fitting curve is also more suitable, indicating that the adsorption process is mainly due to chemical adsorption [29]. Table 2 shows that, under the same impregnation ratio, the adsorption amount of heavy metals obtained by biochar at the final temperature of pyrolysis at 550 °C is greater than the adsorption amount of biochar at 750 °C (1PBC550 > 1PBC750, 2PBC550 > 2PBC750), this is because the increase in the final temperature of pyrolysis leads to a large loss of surface functional groups and the biochar reduces the specific surface, making its heavy metal

adsorption capacity weak; at the same final temperature of pyrolysis, the adsorption amount of high impregnation ratio is greater than the adsorption amount of heavy metals with low impregnation ratio (2PBC550 > 1PBC550, 2PBC750 > 1PBC750) and the adsorption of lead and cadmium exhibits the same law. According to the SSA data, it is visible that the SSA of low-impregnation ratio biochar is higher than that of high-impregnation ratio biochar, but the adsorption experiment results are contrary to the SSA. It is speculated that the SSA is not the key factor affecting the Q_e of biochar, and the successful load of phosphorus-containing functional groups is the main factor to improve the Q_e of phosphorus-modified biochar. The adsorption rate constant K_2 obtained by fitting PSO can reflect the speed of the adsorption process. The larger the value of the kinetic rate constant, the faster the adsorption process is carried out and the shorter the time required to reach equilibrium. From the fitting parameters in the table, it can be seen that the rate constant K_2 of the PSO of 2PBC550 is the largest, indicating that the rate of adsorption of heavy metals by 2PBC550 is the largest, and the equilibrium is reached at the earliest.

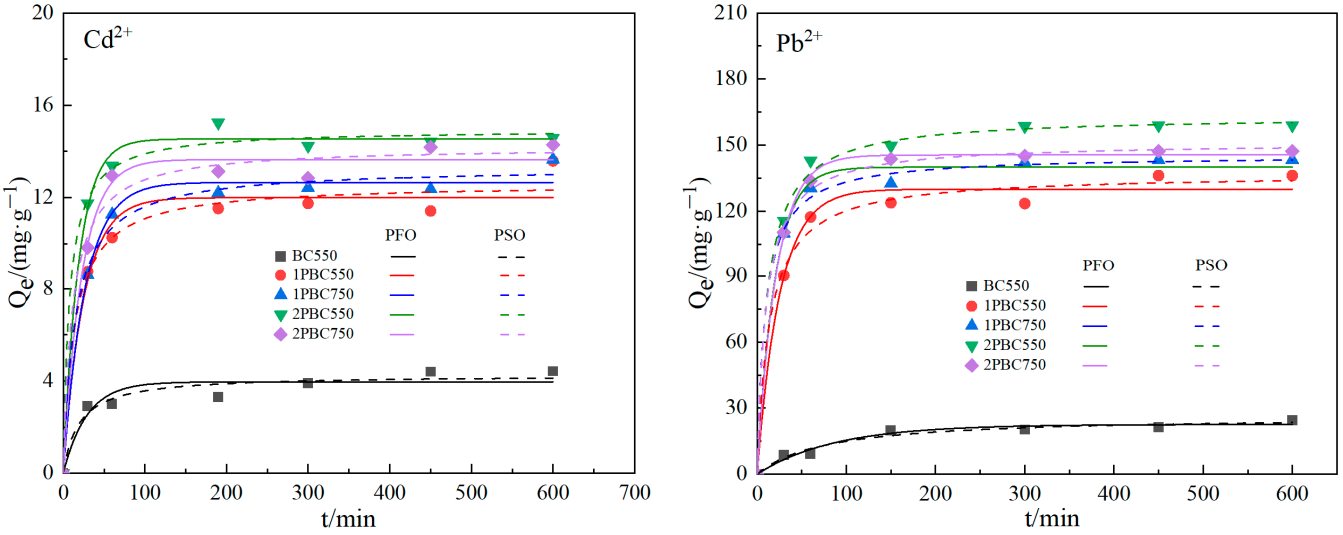

Figure 3. Adsorption kinetics curves of Pb^{2+} and Cd^{2+} by different biochars.

Table 2. Fitting parameters of the PFO and PSO models for the adsorption of Pb^{2+} and Cd^{2+} by different biochars.

		C_0 mg·g^{-1}	PFO				PSO			
			q_e mg·g^{-1}	K_1 h^{-1}	R_{adj}^2	RMSE	q_e mg·g^{-1}	K2 × 10^{-2} mg·g^{-1}h^{-1}	R_{adj}^2	RMSE
Pb^{2+}	BC550	200	22.50	0.988	0.954	1.749	26.50	0.048	0.958	1.669
	1PBC750		129.95	0.962	0.986	5.062	136.91	0.052	0.989	4.519
	1PBC550		139.92	0.951	0.993	3.836	145.35	0.055	0.997	2.691
	2PBC550		145.48	0.954	0.998	3.607	151.17	0.066	0.997	2.819
	2PBC750		139.93	0.952	0.940	3.358	163.24	0.075	0.998	2.404
Cd^{2+}	BC550	20	3.961	0.996	0.898	0.441	4.256	0.436	0.942	0.332
	1PBC750		11.98	0.961	0.963	0.784	12.604	0.576	0.979	0.635
	1PBC550		12.654	0.963	0.988	0.437	13.309	0.509	0.989	0.453
	2PBC550		14.533	0.949	0.993	0.396	14.949	0.875	0.995	0.462
	2PBC750		13.642	0.957	0.986	0.533	13.642	0.623	0.982	0.611

3.2.2. Adsorption Isotherm

The isothermal adsorption curve can be used to study the maximum adsorption capacity of the adsorbent material to the adsorbent, and it reflects the characteristics that the adsorption capacity of the adsorbent material changes with the change of the initial concentration of the adsorbate.

The isothermal adsorption curve can be used to study the maximum adsorption amount of the adsorbate on the adsorbent, and it reflects the characteristics that the adsorption capacity of the adsorbent material changes with the change of the initial concentration of the adsorbate. Figure 4 shows that with the increase of the equilibrium concentration, the adsorption of Pb^{2+} and Cd^{2+} on the biochar gradually increases, the adsorption of phosphorus-modified biochar on Pb^{2+} and Cd^{2+} is significantly higher than unmodified biochar, and the adsorption effect of 2PBC550 is the best.

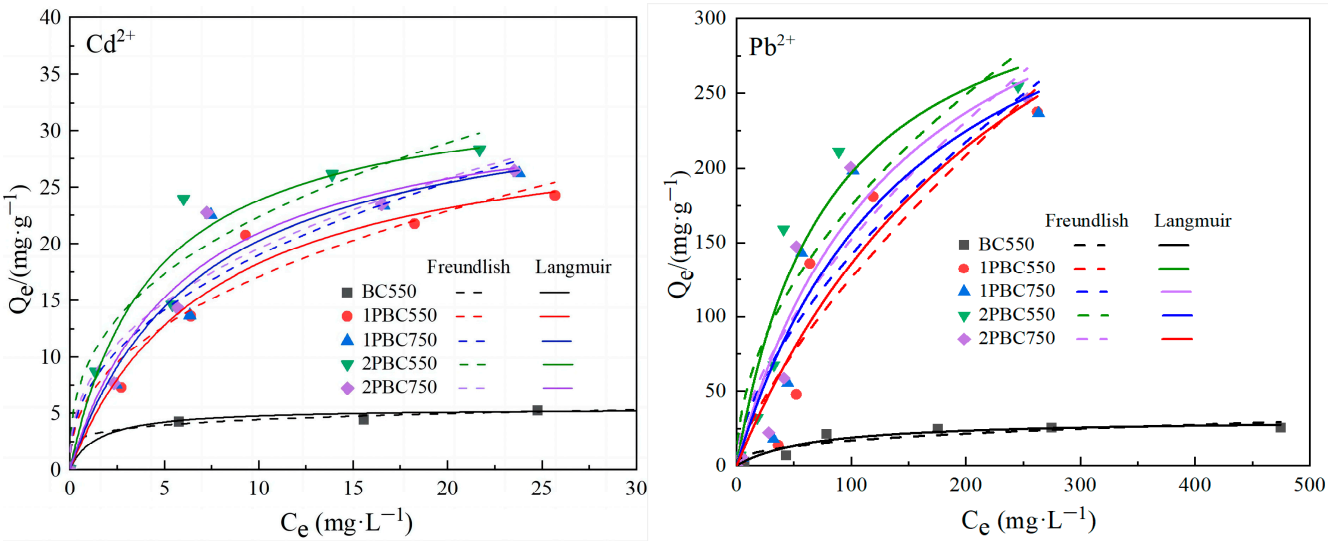

Figure 4. Isothermal adsorption curves of Pb^{2+} and Cd^{2+} by different biochars.

The Langmuir and Freundlich equations were used to fit the adsorption isotherm to compare the adsorption differences of Pb^{2+} and Cd^{2+} after biochar modification. Table 3 shows the result of fitting. From the table data, it can be seen that the RMSE of the Langmuir model is smaller than that of the Freundlich model, indicating that the Langmuir model can better fit the data. At the same time, the correlation coefficient R_{adj}^2 of the Langmuir model is also significantly higher than that of the Freundlich model; so the Langmuir isotherm model can better describe the adsorption process of biochar on Pb^{2+} and Cd^{2+}, and it shows that the adsorption process is single-molecular layer adsorption [30]. Through calculations, it can be concluded that the Q_m of 2PBC550 on Pb^{2+} and Cd^{2+} is 284.171 $mg \cdot g^{-1}$ and 34.154 $mg \cdot g^{-1}$, respectively, compared with unmodified biochar, it is greatly improved. This suggests that modified biochar promotes the adsorption of Pb^{2+} and Cd^{2+}. In addition, the K_L of the Langmuir model represents the affinity between the heavy metal ions in the solution and the adsorbent. The K_L values of 2PBC550 for Pb^{2+} and Cd^{2+} are 0.0125 and 0.2308 $L \cdot mg^{-1}$, respectively. It is significantly higher than other biochar, which indicates that 2PBC550 has a stronger adsorption binding force for Cd^{2+} and Pb^{2+}.

Table 3. Fitting parameters of isothermal adsorption curves for the adsorption of Pb^{2+} and Cd^{2+} by different biochars.

	Biochar	Langmuir Model				Freundlich Model			
		Q_m $mg \cdot g^{-1}$	K_L $L \cdot mg^{-1}$	R_{adj}^2	RMSE	K_F $mg^{-1-N} \cdot g^{-1} \cdot L^{-N}$	N	R_{adj}^2	RMSE
Pb^{2+}	BC550	31.300	0.0149	0.916	3.016	3.208	2.788	0.829	4.301
	1PBC750	223.887	0.0037	0.876	30.756	4.4748	1.379	0.849	34.019
	1PBC550	255.611	0.0066	0.855	34.090	8.3446	1.625	0.804	39.587
	2PBC550	284.171	0.0125	0.913	27.769	16.7185	1.962	0.848	36.716
	2PBC750	279.376	0.0072	0.884	31.203	9.4461	1.657	0.835	37.235
Cd^{2+}	BC550	25.799	0.0994	0.938	1.646	4.0210	2.128	0.975	1.632
	1PBC750	31.723	0.1347	0.964	1.614	6.4303	2.361	0.928	2.264
	1PBC550	33.464	0.1665	0.935	2.371	7.7205	2.482	0.896	2.994
	2PBC550	34.154	0.2308	0.927	2.709	9.5197	2.698	0.905	3.081
	2PBC750	34.090	0.1458	0.922	2.576	7.1397	2.359	0.889	3.083

3.2.3. Competitive Adsorption

The adsorption process of BC550 and 2PBC550 biochar on Pb^{2+} and Cd^{2+} under binary conditions is shown in Figure 5. Figure 5a indicates that when the concentration of Pb^{2+} is used as the background of the fixed concentration, as the concentration of Cd^{2+} increases, the adsorption of unmodified biochar BC to Pb^{2+} can be observed to decrease to a certain extent, indicating that the concentration of Cd^{2+} inhibits the adsorption of BC to Pb^{2+}. The adsorption of Pb^{2+} by the modified biochar (2PBC550) decreased slightly, which was not much different from the adsorption of a single adsorption experiment, and the effect was not obvious. This shows that the modified biochar has played a certain role in alleviating the influence of higher Cd^{2+} concentrations on the adsorption of heavy metals Pb^{2+} by biochar. The influence of adsorption of heavy metal Pb^{2+} has played a certain role. Figure 5b shows that when the concentration of Cd^{2+} is used as the background of the fixed concentration, it can be observed that as the concentration of Pb^{2+} increases, the adsorption of Cd^{2+} by BC550 and 2PBC550 decreases, indicating that there is a competitive relationship between Pb^{2+} and Cd^{2+} in the composite system. Comparing Figure 5a,b, it can be seen that for 2PBC550, Pb^{2+} has a greater impact on Cd^{2+} adsorption, indicating that Pb^{2+} has a higher adsorption priority. Other scholars have obtained similar results, showing that in the dual system—where the heavy metals lead and cadmium coexist—biomass materials are more conducive to the adsorption of lead.

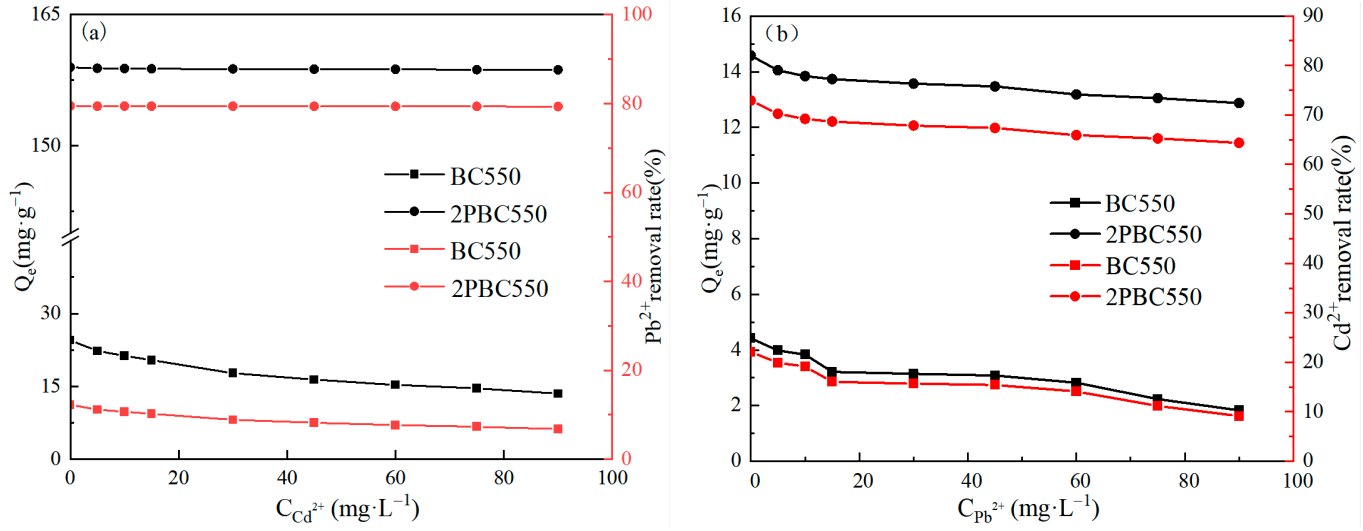

Figure 5. Adsorption of Pb^{2+} (**a**) and Cd^{2+} (**b**) by BC and 2PBC550 biochar under binary conditions.

Whether it is before or after modification, biochar tends to adsorb Pb^{2+} more. The selectivity of competitive adsorption is related to the differences in the chemical properties of heavy metals themselves; such as the relative atomic mass of heavy metals, the hydrolysis constant, and the radius of hydrated ions. On the one hand, the adsorption affinity of metals is proportional to the hydrolysis constant, ion radius, and atomic weight (Pb^{2+} is higher than Cd^{2+}). Therefore, in the competitive adsorption process, the adsorption characteristics of Pb^{2+} are much less affected than Cd^{2+} (this is the same as the experimental results in Figure 5, making Pb^{2+} more susceptible to adsorption reactions; otherwise, the affinity between heavy metal ions and biochar is inversely proportional to the hydration radius of metal ions). It is known that the hydration radius of Pb^{2+} (4.01 Å) is less than Cd^{2+} (4.26 Å), so biochar has a greater impact on Pb^{2+}. The affinity for lead is higher. In addition, the selectivity coefficient of 2PBC550 is higher than that of BC550, indicating that the modified biochar 2PBC550 has a better adsorption capacity than the unmodified biochar BC550 in the binary metal system.

3.2.4. Effect of Initial pH

Figure 6a,b shows the effects of different pH values of the solution on the adsorption of Pb^{2+} and Cd^{2+}, respectively. It can be seen from the figure that the adsorption capacity of 2PBC550 to Pb^{2+} and Cd^{2+} reaches its maximum value at a pH of 5, which is 145.48 $mg \cdot g^{-1}$ and 14.771 $mg \cdot g^{-1}$, respectively. At low pH, the H^+ and metal ions in the solution will compete for the surface site of the adsorbent, resulting in a poor adsorption effect [31]. As the pH continues to increase, it can be observed that the adsorption of Pb^{2+} by BC550 and 2PBC550 decreases. This is because there is too much precipitation by OH- in the solution, which inhibits the adsorption capacity of Pb^{2+}; while the adsorption capacity of Cd^{2+} decreases slightly.

Figure 6c,d shows the dominant species of Pb^{2+} and Cd^{2+} predicted using Visual MINTEQ 3.1 under specific experimental conditions. The results show that under the pH value we set, precipitation such as $Pb(OH)_2(aq)$, $CdOH^+$ and $Cd(OH)_2(aq)$ are not dominant species, which fully shows that the removal of Pb^{2+} and Cd^{2+} mainly depends on adsorption rather than hydroxide precipitation; this is consistent with the previous research results [32].

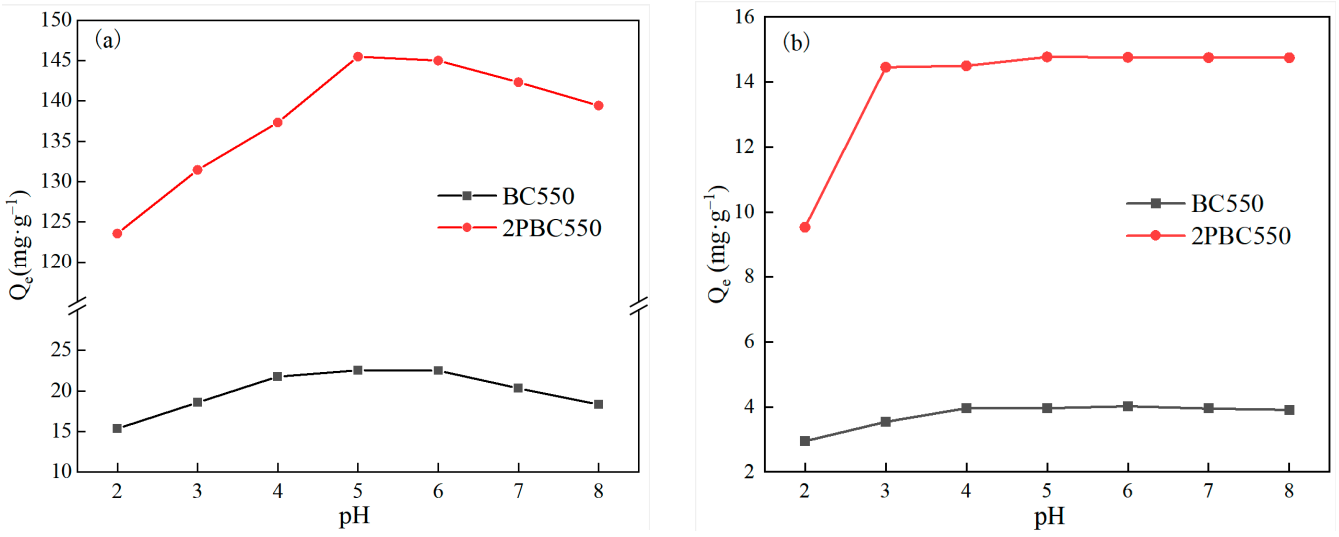

Figure 6. *Cont.*

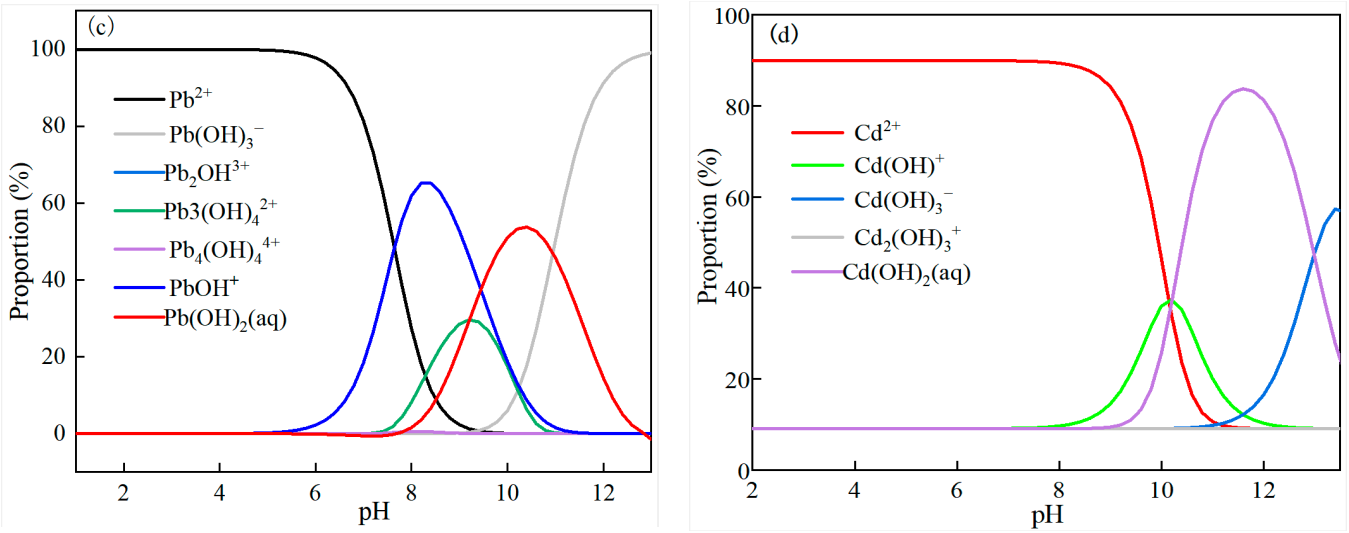

Figure 6. Effect of biochar on the adsorption of Pb^{2+} (**a**) andCd^{2+} (**b**) under different pH conditions and the forms of Pb^{2+} (**c**) and Cd^{2+} (**d**) at different pH.

3.3. Mechanism Analysis

3.3.1. FTIR and XRD

As shown in Figure 7a,c, through FTIR technology, we observed that the functional groups of biochar changed after adsorption of Pb^{2+} and Cd^{2+}, and the intensity of the -OH peak decreased. This is mainly because during the adsorption process, Cd-O/Pb-O complexes are generated or $Cd(OH)_2$ and $Pb(OH)_2$ are deposited on the surface of the biochar. Simultaneously, the characteristic peaks of -COOH at the 1560 cm^{-1} position and C-O at the 1086 cm^{-1} position also decreased in strength after adsorption of heavy metals, indicating that -COOH and C-O are also involved in the adsorption of Pb^{2+} and Cd^{2+}. Compared with the uncorbed Pb^{2+} and Cd^{2+} biochar in Figure 2a, the PO_4^{3-} characteristic peak intensity of the phosphorus-modified biochar located at 960 cm^{-1} and 538 cm^{-1} after adsorption of Pb^{2+} and Cd^{2+} was significantly weakened, indicating that Pb^{2+} and Cd^{2+} reacted with PO_4^{3-} to form a precipitate; the P-O-P characteristic peak intensity in the 692–890 cm^{-1} region decreased, indicating that $P_2O_7^{4-}$ interacted with Pb^{2+} and Cd^{2+} to form $Pb_2P_2O_7/Cd_2P_2O_7$. The comparison also found that the phosphorus-containing functional group of 2PBC550 even disappeared, indicating that there is a significant interaction between heavy metals and phosphorus-containing functional groups; this explains why 2PBC550 has a better adsorption effect than 2PBC750. In summary, the -OH, -COOH, C-O groups and P-containing groups participate in the reaction of surface complexation and precipitation adsorption of Pb^{2+} and Cd^{2+}.

As shown in Figure 7b,d, the crystal structure of biochar after adsorption of Pb^{2+} and Cd^{2+} was analyzed by XRD. As shown in Figure 7b, the XRD diagram after adsorption of Pb^{2+}, it is found that biochar forms Pb^{2+} containing compounds. For example, 2PBC550 has $Pb_3(PO_4)_2$ new characteristic peaks at 30.4°, 43.3° and 49.0°; and $Pb_2P_2O_7$ characteristic peaks at 22.1°, 26.1° and 27.8°, which fully demonstrates that the phosphorus-containing group on the surface of 2PBC550 reacts with Pb^{2+} to form $Pb_3(PO_4)_2$ and $Pb_3(PO_4)_2$. Precipitation of $Pb_2P_2O_7$, in addition, a small number of $Pb(OH)_2$ diffraction peaks appeared at a position of about 45.5°. In Figure 7d, the XRD diagram after adsorption of Cd^{2+}, biochar 2PBC550 has a new peak at 36.3° and 38.2°, which correspond well to $Cd_2P_2O_7$ and $Cd_3(PO_4)_2$, respectively. At the same time, a small amount of $Cd(OH)_2$ precipitation was also found. According to the XRD atlas analysis, it can be seen that phosphate precipitation was found after the biochar 2PBC550 adsorbed Pb^{2+} and Cd^{2+}, indicating that the main mechanism of adsorption of heavy metals is to rely on the phosphorus-containing groups loaded on the surface of the biochar to react with heavy metals and exist on the

surface of the biochar in the form of phosphate precipitation, which matches with the FT-IR analysis results.

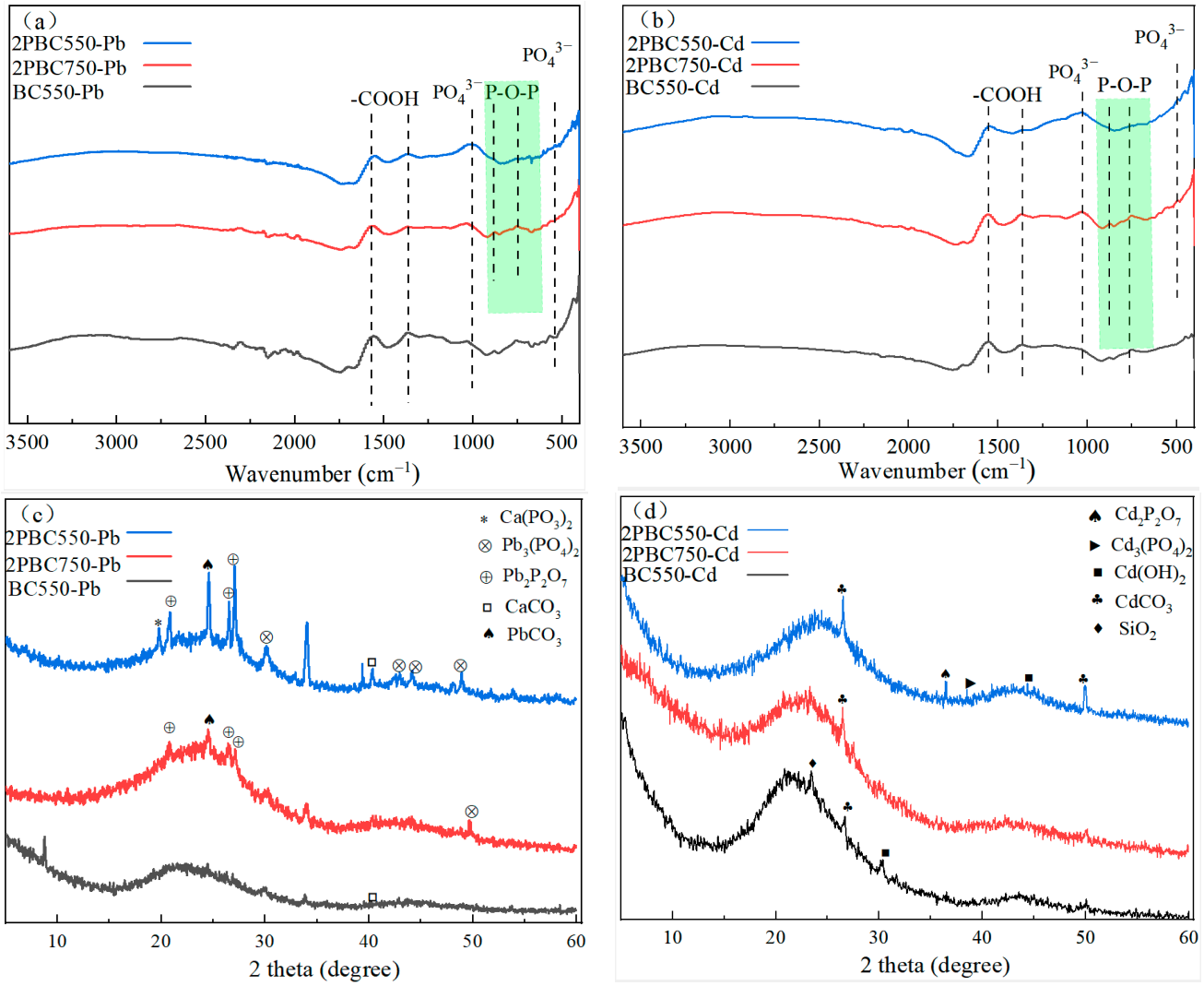

Figure 7. Infrared spectra (**a**,**c**) and XRD spectra (**b**,**d**) after adsorption of Pb^{2+} and Cd^{2+} by different biochars.

3.3.2. XPS Analysis

Whole-spectrum changes in unmodified biochar and phosphorus-modified biochar (2PBC550, 2PBC750) before and after adsorption of Pb^{2+} and Cd^{2+} were analyzed using XPS, as shown in Figure 8a. From the figure, the two conspicuous peaks of O1s (532.08 eV) and C1s (285.06 eV) can be clearly seen. Compared with the unmodified biochar BC550, the modified biochars 2PBC550 and 2PBC750 have the characteristic peak of P 2p at 134.5 ev; and the peak intensity of C1s is weakened, and the peak intensity of O1s is enhanced, indicating that the phosphorus-containing group has been successfully loaded on the modified biochar. After adsorption of heavy metals, the characteristic peaks of Pb4f and Pb4d appeared at about 139.08 eV and 414.6 eV; in addition, the characteristic peaks of Cd3d3/2 and Cd3d5/2 appeared at 406 eV and 414 eV, indicating that biochar successfully adsorbed Pb^{2+} and Cd^{2+}.

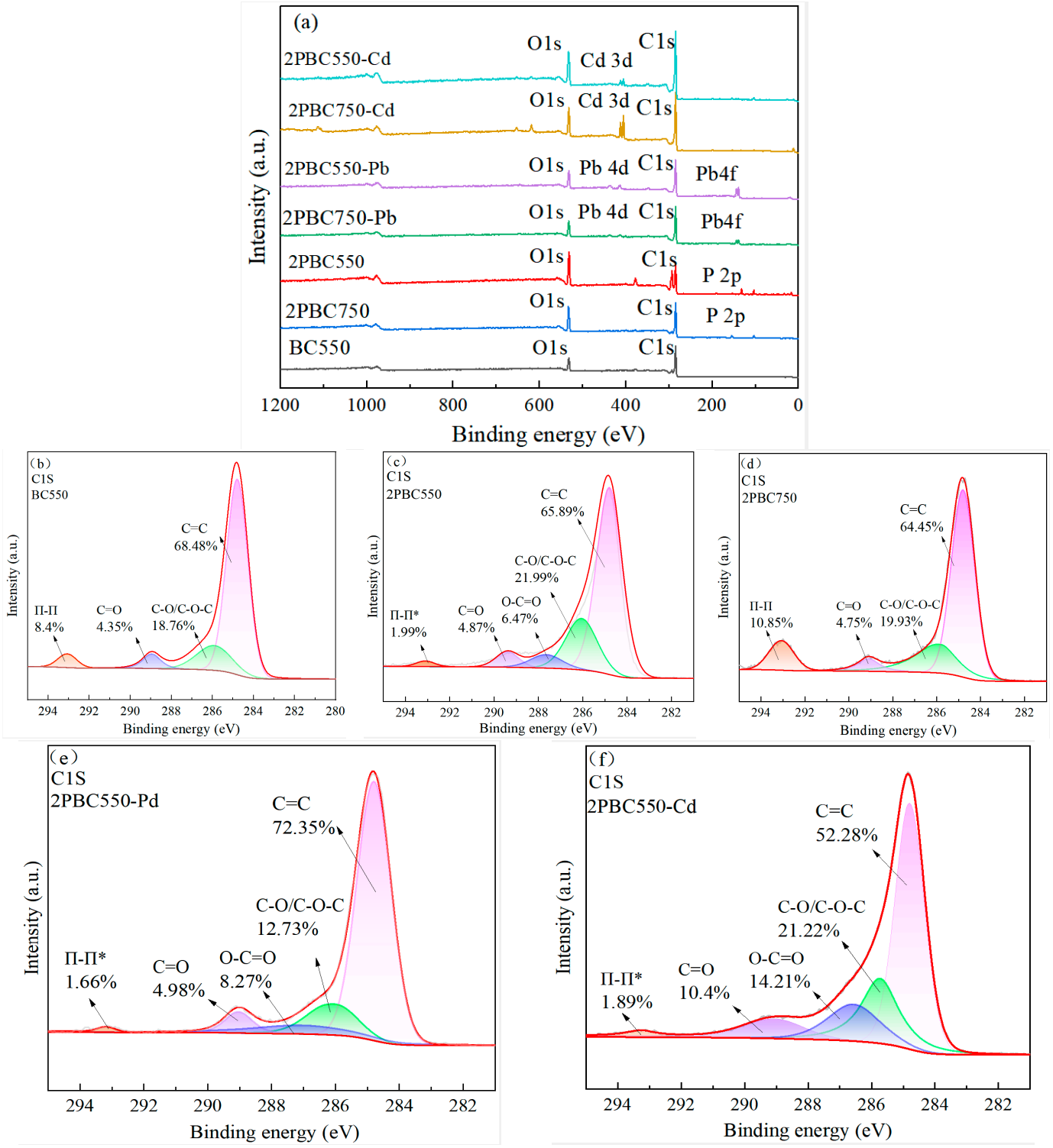

Figure 8. *Cont.*

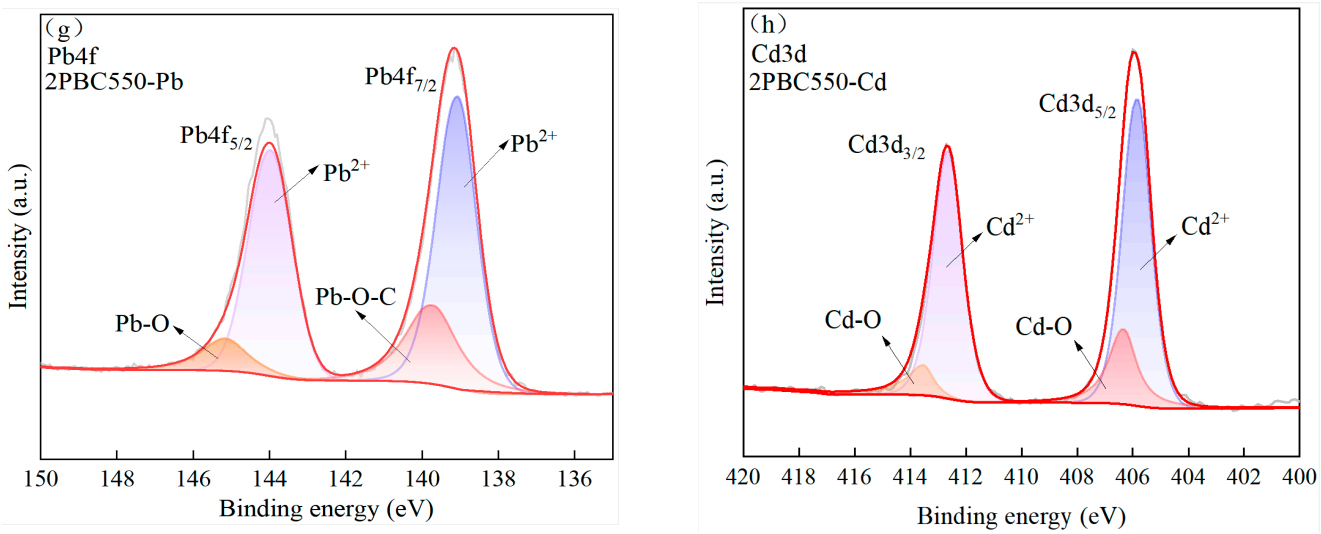

Figure 8. XPS spectrum before and after adsorption of Pb^{2+} and Cd^{2+} by different biochar (**a**) and C1S patterns of Pb^{2+} and Cd^{2+} adsorption by different biochar (**b**–**f**). Pb4f, Cd3d (**g**,**h**) plots of 2PBC550 biochar.

Figure 8b–d shows the C1S map of unmodified biochar and modified biochar (2PBC550, 2PBC750). In the C1s spectrum, located at 284.8 eV, 286 ± 0.3 eV and 288.5 ± 0.3 eV, correspond to C-C, C-O/C-O-C, and C=O, respectively. The peak area of the phosphorus-modified biochar at C-O/C-O-C C=O increased significantly, which shows that the phosphorus modification can add oxygen-containing functional groups to the surface of the biochar. Therefore, the ability of the modified biochar to form complexes with Pb^{2+} and Cd^{2+} is better than that of the unmodified biochar, which is suitable for the previous research results [33]. By comparing Figure 8c,d, it was found that a significant peak appeared at 287.65 eV on the C1s spectrum of 2PBC550 biochar, which corresponds well to the characteristic peak of C-O=C. This indicates that the content of oxygenated functional groups in the improved biochar 2PBC550 exceeds that of 2PBC750. This implies that the higher pyrolysis final temperature is not favorable for the retention of the oxygenated functional groups, which directly leads to a reduction in its ability to complex with the heavy metals; which in turn affects the performance of the biochar and further leads to the reduction of adsorption of 2PBC750 [34]. As shown in Figure 8e, the C1S map of the modified biochar 2PBC550 after adsorbing the heavy metal Pb^{2+}, during the adsorption process it can be seen that the content of C-O/C-O-C has dropped from 21.99% to 12.73%, indicating that C-O/C-O-C has a certain consumption. It is speculated that it may be because in the process of forming a Pb-O complex, electrons are transferred from the surface of the O atom to the surface of the Pb^{2+}, and the content of C=O and C-O=C increased from 4.87% to 4.98%, and increased from 6.47% to 8.27%. It is speculated that the increase in C=O content may be owing to the newly formed carbonate; that is, C=O in $PbCO_3$. As shown in Figure 8f, the C1S map of the modified biochar 2PBC550 after adsorbing the heavy metal Cd^{2+} is similar to the C1S map of the adsorbed Pb^{2+}. During the adsorption process, the content of C-O/C-O-C decreased from 21.99% to 21.22%, indicating that the consumption of C-O, while the content of C=O and C-O=C increased from 4.87% to 14.21% and from 6.47% to 10.4%. It fully explains that the C-O and C=O on the surface of 2PBC550 are used in cooperation with the occurrence networks of Pb^{2+} and Cd^{2+}, which is consistent with the FTIR results [32]. At the same time, we found that the content of C=C decreases after adsorption of Cd^{2+}, indicating that in the ion exchange between biochar and metal Cd^{2+}, the aromatic structure of biochar provides π electrons, which participates in the adsorption process of Cd^{2+} to form a metal π complex, and the content of π-π* is found to decrease.

The Pb4f spectrum of 2PBC550 adsorbing Pb^{2+} can be seen in Figure 8g. At 139.14 eV and 144.01 eV are the two peaks of Pb4f7/2 and Pb4f5/2, respectively, which are the

excitation peaks of Pb-O-C and Pb-O, which can be attributed to $PbCO_3$ and $Pb_3(PO_4)_2$. The peaks at 140.01 eV and 145.16 eV indicate that Pb^{2+} reacts with oxygen-containing functional groups on the surface of the material to form. Pb-O/$Pb(OH)_2$ complex. The spectrum of Cd3d adsorbed by 2PBC550 Cd^{2+} is shown in Figure 8h. From the figure, we found that Cd3d5/2 and Cd3d3/2 appear at 405.82 eV and 412.63 eV, respectively. These are due to $CdCO_3$ and $Cd_3(PO_4)_2$. In addition, additional peaks appeared at 407.14 eV and 414.11 eV, indicating that the oxygen-containing functional group on the surface of the biochar material reacted with Cd^{2+} to form a Cd-O/$Cd(OH)_2$ complex. This showed the active role of oxygen-containing functional groups in adsorption. The XPS results confirm each other with the results of FTIR and XRD in the previous article, indicating that the main adsorption mechanism of biochar 2PBC550 for heavy metals (Pb^{2+} and Cd^{2+}) after phosphorus modification is complexation and precipitation.

4. Conclusions

In this paper, through the exploration of different temperatures and the proportion of modifiers added to corn stalk biochar, we discovered that the modified biochar showed a significantly improved effect on the adsorption of heavy metal ions Pb^{2+} and Cd^{2+}. In particular, the modified biochar 2PBC550 showed the best adsorption performance, and its maximum adsorption capacity was 284.171 $mg \cdot g^{-1}$ and 34.154 $mg \cdot g^{-1}$, respectively. Comparison with the adsorption capacity of biochar in other related literature shows that the 2PBC550 in this study showed relatively excellent adsorption performance (Table S4). This discovery is of great significance for the effective utilization of corn stalk biomass resources and the treatment of heavy metal pollutants, and provides a useful reference for future environmental protection and sustainable use of resources.

Meanwhile, the results show that the quasi-secondary dynamics and Langmuir isothermal models simulate well the adsorption process of Pb^{2+} and Cd^{2+} of biochar after modification, indicating that the adsorption process is dominated by single-layer chemical adsorption.

In the binary metal composite system, Pb^{2+} is adsorbed preferentially than Cd^{2+}, but 2PBC550 weakens the inhibitory effect of Pb^{2+} on Cd^{2+} adsorption in the meta-metal composite system to a certain extent. Through characterization, it was found that phosphorus-based biochar (2PBC550) has a higher surface area and more hydroxyl and carboxyl groups, and successfully loaded phosphorus-containing functional groups. Mechanism analysis shows that the adsorption mechanism of phosphorus-based biochar to heavy metals (Pb^{2+} and Cd^{2+}) is mainly caused by the precipitation of phosphorus-containing groups and the complexation caused by oxygen-containing functional groups on the carbon surface.

In summary, phosphorus-based biochar (2PBC550) can be regarded as an adsorbent that effectively removes Pb^{2+} and Cd^{2+} from wastewater, and provides a simple and feasible solution for the scientific utilization of corn stalk waste materials for resource utilization and the repair of heavy metal contaminated water bodies.

Supplementary Materials: The following supporting information can be downloaded at: https://www.mdpi.com/article/10.3390/agriculture14071118/s1, Figure S1: adsorption of Pb^{2+} and Cd^{2+} by unmodified biochar at different pyrolysis temperatures; Table S1: list of experimental reagents; Table S2: experimental data of adsorption dynamics; Table S3: effect of different pH on adsorption volume; Table S4: The comparison of maximum adsorption capacities of different biochars for Pb^{2+} or Cd^{2+} [35–39].

Author Contributions: Conceptualization, L.Z. and Z.L.; methodology, L.Z. and L.C. (Lin Chen); software, L.C. (Lin Chen) and Y.Z. (Yu Zhang); validation, L.C. (Lin Chen); formal analysis, Y.Z. (Yuqing Zhang), Z.L. and K.Y.; investigation, Y.Z. (Yuqing Zhang), Y.Z. (Yu Zhang) and K.Y.; resources, L.Z. and L.C. (Limei Chen); data curation, Y.Z. (Yuqing Zhang) and Z.L.; writing—original draft preparation, L.C. (Lin Chen) and K.Y.; writing—review and editing, L.Z. and L.C. (Limei Chen); visualization, L.C. (Lin Chen); supervision, L.Z., Y.Z. (Yuqing Zhang) and L.C. (Limei Chen); project administration, L.C. (Limei Chen); funding acquisition, L.C. (Limei Chen). All authors have read and agreed to the published version of the manuscript.

Funding: This research was funded by the Key R&D Project of Jilin Provincial Science and Technology Department (20230203172SF).

Institutional Review Board Statement: Not applicable.

Data Availability Statement: Some data are available upon reasonable request from the corresponding author.

Acknowledgments: We are very grateful for the support of the research and application project of soil environmental restoration technology for facility cultivation.

Conflicts of Interest: The authors declare no conflicts of interest.

References

1. Kaushik, P.; Khandelwal, R.; Rawat, N.; Sharma, M.K. Environmental hazards of heavy metal pollution and toxicity: A review. *Flora Fauna* **2022**, *28*, 315–327. [CrossRef]
2. Peng, H.B.; Gao, P.; Chu, G.; Pan, B.; Peng, J.H.; Xing, B.S. Enhanced adsorption of Cu (II) and Cd (II) by phosphoric acid-modified biochars. *Environ. Pollut.* **2017**, *229*, 846–853. [CrossRef]
3. Wang, J.W.; Zhang, Y.S.; Liu, Z.; Gu, Y.Z.; Norris, P.; Xu, H.; Pan, W.P. Coeffect of air pollution control devices on trace element emissions in an ultralow emission coal-fired power plant. *Energy Fuels* **2019**, *33*, 248–256. [CrossRef]
4. Jiang, Q.; Xie, W.L.; Han, S.Y.; Wang, Y.F.; Zhang, Y. Enhanced adsorption of Pb (II) onto modified hydrochar by polyethyleneimine or H_3PO_4: An analysis of surface property and interface mechanism. *Colloid Surf. A* **2019**, *583*, 123962. [CrossRef]
5. Liu, X.J.; Lai, D.G.; Wang, Y. Performance of Pb (II) removal by an activated carbon supported nanoscale zero-valent iron composite at ultralow iron content. *J. Hazard. Mater.* **2019**, *361*, 37–48. [CrossRef]
6. Hopkins, D.; Hawboldt, K. Biochar for the removal of metals from solution: A review of lignocellulosic and novel marine feedstocks. *J. Environ. Chem. Eng.* **2020**, *8*, 103975. [CrossRef]
7. Zhou, Y.W.; Qin, S.Y.; Verma, S.; Sar, T.; Sarsaiya, S.; Ravindran, B.; Liu, T.; Sindhu, R.; Patel, A.K.; Binod, P. Production and beneficial impact of biochar for environmental application: A comprehensive review. *Bioresour. Technol.* **2021**, *337*, 125451. [CrossRef]
8. Li, B.; Yang, L.; Wang, C.Q.; Zhang, Q.P.; Liu, Q.C.; Li, Y.D.; Xiao, R. Adsorption of Cd (II) from aqueous solutions by rape straw biochar derived from different modification processes. *Chemosphere* **2017**, *175*, 332–340. [CrossRef] [PubMed]
9. Sizmur, T.; Fresno, T.; Akgül, G.; Frost, H.; Moreno-Jiménez, E. Biochar modification to enhance sorption of inorganics from water. *Bioresour. Technol.* **2017**, *246*, 34–47. [CrossRef] [PubMed]
10. Yang, J.P.; Zhao, Y.C.; Ma, S.M.; Zhu, B.B.; Zhang, J.Y.; Zheng, C.G. Mercury removal by magnetic biochar derived from simultaneous activation and magnetization of sawdust. *Environ. Sci. Technol.* **2016**, *50*, 12040–12047. [CrossRef]
11. Bakshi, S.; Banik, C.; Rathke, S.J.; Laird, D.A. Arsenic sorption on zero-valent iron-biochar complexes. *Water Res.* **2018**, *137*, 153–163. [CrossRef] [PubMed]
12. Son, E.B.; Poo, K.M.; Chang, J.S.; Chae, K.J. Heavy metal removal from aqueous solutions using engineered magnetic biochars derived from waste marine macro-algal biomass. *Sci. Total Environ.* **2018**, *615*, 161–168. [CrossRef]
13. Martinez, C.E.; Jacobson, A.R.; Astrid, R.; Mcbride, M.B. Lead phosphate minerals: Solubility and dissolution by model and natural ligands. *Environ. Sci. Technol.* **2004**, *38*, 5584–5590. [CrossRef] [PubMed]
14. Tan, X.F.; Liu, Y.G.; Gu, Y.L.; Xu, Y.; Zeng, G.M.; Hu, X.J.; Liu, S.B.; Wang, X.; Liu, S.M.; Li, J. Biochar-based nano-composites for the decontamination of wastewater: A review. *Bioresour. Technol.* **2016**, *212*, 318–333. [CrossRef]
15. Zhang, S.H.; Zhang, H.; Cai, J.; Zhang, X.; Zhang, J.J.; Shao, J.A. Evaluation and prediction of cadmium removal from aqueous solution by phosphate-modified activated bamboo biochar. *Bioresour. Technol.* **2018**, *32*, 4469–4477. [CrossRef]
16. Gao, R.L.; Fu, Q.L.; Hu, H.Q.; Wang, Q.; Liu, Y.H.; Zhu, J. Highly-effective removal of Pb by co-pyrolysis biochar derived from rape straw and orthophosphate. *J. Hazard. Mater.* **2019**, *371*, 191–197. [CrossRef]
17. Zhou, N.; Chen, H.G.; Feng, Q.J.; Yao, D.H.; Chen, H.L.; Wang, H.Y.; Zhou, Z.; Li, H.Y.; Tian, Y.; Lu, X.Y. Effect of phosphoric acid on the surface properties and Pb (II) adsorption mechanisms of hydrochars prepared from fresh banana peels. *J. Clean Prod.* **2017**, *165*, 221–230. [CrossRef]
18. Zhang, H.; Shao, J.G.; Zhang, S.H.; Zhang, X.; Chen, H.P. Effect of phosphorus-modified biochars on immobilization of Cu (II), Cd (II), and As (V) in paddy soil. *J. Hazard. Mater.* **2020**, *390*, 121349. [CrossRef]
19. Egüés, I.; Sanchez, C.; Mondragon, I.; Labidi, J. Effect of alkaline and autohydrolysis processes on the purity of obtained hemicelluloses from corn stalks. *Bioresour. Technol.* **2012**, *103*, 239–248. [CrossRef]
20. Yakout, S.M. Physicochemical characteristics of biochar produced from rice straw at different pyrolysis temperature for soil amendment and removal of organics. *Proc. Natl. Acad. Sci. India A* **2017**, *87*, 207–214. [CrossRef]
21. Zhang, J.H.; Huang, B.; Chen, L.; Li, Y.; Li, W.; Luo, Z.X. Characteristics of biochar produced from yak manure at different pyrolysis temperatures and its effects on the yield and growth of highland barley. *Chem. Spec. Bioavailab.* **2018**, *30*, 57–67. [CrossRef]

22. Chen, Y.N.; Zeng, Z.P.; Li, Y.P.; Liu, Y.H.; Chen, Y.R.; Wu, Y.X.; Zhang, J.C.; Li, H.; Xu, R.; Wang, S. Glucose enhanced the oxidation performance of iron-manganese binary oxides: Structure and mechanism of removing tetracycline. *J. Colloid Interface Sci.* **2020**, *573*, 287–298. [CrossRef] [PubMed]
23. Li, K.; Zhang, Z.X.; Ma, S.W.; Ma, S.W.; Wang, B.; Cui, M.S.; Lu, Q.; Yang, Y.P. Effects of $NH_4H_2PO^4$-loading and temperature on the two-stage pyrolysis of biomass: Analytical pyrolysis-gas chromatography/mass spectrometry study. *J. Biobased Mater. Bioenergy* **2020**, *14*, 76–82. [CrossRef]
24. Chen, Y.N.; Li, M.L.; Li, Y.P.; Liu, Y.H.; Chen, Y.R.; Li, H.; Li, L.S.Z.; Xu, F.T.; Jiang, H.J.; Chen, L. Hydroxyapatite modified sludge-based biochar for the adsorption of Cu^{2+} and Cd^{2+}: Adsorption behavior and mechanisms. *Bioresour. Technol.* **2021**, *321*, 124413. [CrossRef] [PubMed]
25. Gao, R.L.; Hu, H.Q.; Fu, Q.L.; Li, Z.H.; Xing, Z.Q.; Ali, U.; Zhu, J.; Liu, Y.H. Remediation of Pb, Cd, and Cu contaminated soil by co-pyrolysis biochar derived from rape straw and orthophosphate: Speciation transformation, risk evaluation and mechanism inquiry. *Sci. Total Environ.* **2020**, *730*, 139119. [CrossRef] [PubMed]
26. Wang, Q.; Duan, C.J.; Xu, C.Y.; Geng, Z.C. Efficient removal of Cd (II) by phosphate-modified biochars derived from apple tree branches: Processes, mechanisms, and application. *Sci. Total Environ.* **2022**, *819*, 152876. [CrossRef]
27. Xu, G.; Zhang, Y.; Shao, H.B.; Sun, J.N. Pyrolysis temperature affects phosphorus transformation in biochar: Chemical fractionation and 31P NMR analysis. *Sci. Total Environ.* **2016**, *569*, 65–72. [CrossRef] [PubMed]
28. Zimmermann, A.C.; Mecabô, A.; Fagundes, T.; Rodrigues, C.A. Adsorption of Cr (VI) using Fe-crosslinked chitosan complex (Ch-Fe). *J. Hazard. Mater.* **2010**, *179*, 192–196. [CrossRef]
29. Çelekli, A.; Ilgün, G.; Bozkurt, H. Sorption equilibrium, kinetic, thermodynamic, and desorption studies of Reactive Red 120 on Chara contraria. *Chem. Eng. J.* **2012**, *191*, 228–235. [CrossRef]
30. Feng, J.; Zou, L.Y.; Wang, Y.T.; Li, B.W.; He, X.F.; Fan, Z.J.; Ren, Y.M.; Lv, Y.Z.; Zhang, M.L.; Chen, D. Synthesis of high surface area, mesoporous MgO nanosheets with excellent adsorption capability for Ni (II) via a distillation treating. *J. Colloid Interface Sci.* **2015**, *438*, 259–267. [CrossRef]
31. Zhang, L.M.; Ren, Y.F.; Xue, Y.H.; Cui, Z.W.; Wei, Q.H.; Han, C.; He, J.Y. Preparation of biochar by mango peel and its adsorption characteristics of Cd (II) in solution. *RSC Adv.* **2020**, *59*, 35878–35888. [CrossRef]
32. Xiao, J.; Hu, R.; Chen, G.C. Micro-nano-engineered nitrogenous bone biochar developed with a ball-milling technique for high-efficiency removal of aquatic Cd(II), Cu(II) and Pb (II). *J. Hazard. Mater.* **2020**, *387*, 121980. [CrossRef] [PubMed]
33. Ding, W.C.; Dong, X.L.; Ime, I.M.; Gao, B.; Ma, L.Q. Pyrolytic temperatures impact lead sorption mechanisms by bagasse biochars. *Chemosphere* **2014**, *105*, 68–74. [CrossRef] [PubMed]
34. Tan, G.Q.; Xiao, D. Adsorption of cadmium ion from aqueous solution by ground wheat stems. *J. Hazard. Mater.* **2009**, *164*, 1359–1363. [CrossRef]
35. Chen, H.Y.; Yang, X.J.; Liu, Y.L.; Lin, X.M.; Wang, J.J.; Zhang, Z.; Li, N.; Li, Y.T.; Zhang, Y.L. KOH modification effectively enhances the Cd and Pb adsorption performance of N-enriched biochar derived from waste chicken feathers. *Waste Manag.* **2021**, *130*, 82–92. [CrossRef] [PubMed]
36. Chen, H.Y.; Li, W.Y.; Wang, J.J.; Xu, H.J.; Liu, Y.L.; Zhang, Z.; Li, Y.T.; Zhang, Y.L. Adsorption of cadmium and lead ions by phosphoric acid-modified biochar generated from chicken feather: Selective adsorption and influence of dissolved organic matter. *Bioresour. Technol.* **2019**, *292*, 121948. [CrossRef] [PubMed]
37. Qin, H.J.; Shao, X.H.; Shaghaleh, H.; Gao, W.; Hamoud, Y.A. Adsorption of Pb^{2+} and Cd^{2+} in Agricultural Water by Potassium Permanganate and Nitric Acid-Modified Coconut Shell Biochar. *Agronomy* **2023**, *13*, 1813. [CrossRef]
38. Chen, Z.L.; Zhang, J.Q.; Huang, L.; Yuan, Z.H.; Li, Z.J.; Liu, M.C. Removal of Cd and Pb with biochar made from dairy manure at low temperature. *J. Integr. Agric.* **2019**, *18*, 201–210. [CrossRef]
39. Zhang, C.H.; Yang, D.S.; Liu, W.; Dong, Y.B.; Zhang, L.P.; Lin, H. Insight into the impacts of pyrolysis time on adsorption behavior of Pb^{2+} and Cd^{2+} by Mg modified biochar: Performance and modification mechanism. *Environ. Res.* **2023**, *239*, 117215. [CrossRef]